



MODELLING CANDU FUEL ELEMENT AND BUNDLE BEHAVIOUR FOR IN- AND OUT-REACTOR PERFORMANCE OF INTACT AND DEFECTIVE FUEL

K. Shaheen*, A.D. Quastel, J.S. Bell, B.J. Lewis, W.T. Thompson, and E.C. Corcoran

Department of Chemistry and Chemical Engineering

Royal Military College of Canada

17000 Station Forces, Kingston, Ontario, Canada K7K 7B4

*Corresponding Author: Tel – 613 541 6000 x 6147, E-mail – Khaled.Shaheen@rmc.ca

ABSTRACT – A proposed platform-based fuel performance code integrates treatments for intact fuel performance and defective fuel oxidation. The intact fuel performance code is verified against the ELESTRES and ELESIM industry-standard toolset for heat transport, fission gas diffusion, and deformation and interaction of the pellet and sheath. The oxidation model integrates equilibrium thermodynamics into oxygen transport equations and is validated against coulometric titration data from Chalk River Laboratories. Ongoing work aims to incorporate the intact fuel performance model into a bundle heat transport and deformation model, and to apply the oxidation to the design and analysis of an out-reactor instrumented fuel oxidation experiment.

1. Introduction

Industry codes such as ELESTRES, ELOCA, and BOW are used to simulate fuel behaviour. The goal of the current work is to test the ability of platform-based models as tools to predict fuel performance and design fuel behavior experiments.

Nuclear fuel performance in an individual element is dependent on a number of inter-related phenomena, including fission heating and heat transport, fission gas release from the evolving uranium dioxide fuel grains and diffusion to the fuel-to-sheath gap, and material deformation of both the fuel and the Zircaloy sheath. Bundle behavior involves the bowing of individual elements, which is primarily thermally induced [1,2], as well as the effects of contact between different elements and the elements and the bundle endplates. With the rare incidence of a sheath defect, coolant flow into the fuel element results in fuel oxidation, which in turn affects the fission gas release from the fuel element [3] and the fuel thermal performance [4].

2. Model Development

Three models are described in this work: (i) A single-element fuel performance code is developed to account for heat and mass transport for intact fuel analysis (Section 2.1); (ii) a bowing model is further considered, based on a beam approximation, to predict the overall deflection of an element due to an external load (Section 2.2); and (iii) a defective fuel oxidation model is applied to simulate fuel oxidation behavior in a proposed out-reactor loop experiment at the Stern Laboratories (Section 2.3). The latter out-reactor loop test is proposed to help validate a previously-developed fuel oxidation model that can be eventually used and implemented in the fuel performance code in order to mechanistically predict defective fuel element behavior. The fuel performance and fuel oxidation models specifically advance the work of Morgan [5] and Higgs et. al. [6], respectively.



The overall objective of the current work is to develop these models on a commercial numerical platform (COMSOL Multiphysics) so that the individual phenomena/codes describing fuel element performance, fuel element/bundle bowing, and defective fuel behaviour can be linked into a single multiphysics tool.

2.1 Intact fuel element performance model

2.1.1 Heat generation and transport

The heat conduction equation in the fuel element is:

$$\rho C_p \frac{\partial T}{\partial t} = \nabla \cdot (k \nabla T) + \frac{P_{lin}}{\pi a_p^2} \left[\frac{\kappa a_p}{2I_1(\kappa a_p)} \right] \times [I_0(\kappa r) + 0.6247 \exp(83.9187(r - a_p))] \quad (1)$$

where r is the radial coordinate, t is time, and T is temperature. The heat generation due to fission is given by the term $\frac{P_{lin}}{\pi a_p^2} \left[\frac{\kappa a_p}{2I_1(\kappa a_p)} \right] \times [I_0(\kappa r) + 0.6247 \exp(83.9187(r - a_p))]$, where P_{lin} is the element power rating (kW m⁻¹), a_p is the pellet radius, κ is the inverse neutron diffusion length, the Bessel functions I_0 and I_1 account for neutron flux depression, and the term $0.6247 \exp(83.9187(r - a_p))$ accounts for the buildup of plutonium on the outer surface of the fuel for an average burnup of 100 MWh kgU⁻¹. The heat generation term applies within the fuel pellet but not in the sheath. The terms ρ , C_p , and k represent density, heat capacity, and thermal conductivity, which vary between the fuel and sheath as shown in Section 3.

Over time, fuel expansion and sheath creepdown bring the fuel and sheath into contact. Due to surface roughness, heat transfer from the fuel pellet to the sheath occurs via both gas conduction and solid-to-solid conduction, for which the coefficients are:

$$h_{solid} = \frac{k_m P_i^{1/2}}{a_0 R_{rms}^{1/2} H} \quad (2)$$

$$h_{gas} = \frac{k_f}{1.5(R_1 + R_2) + t_g + g \left(\frac{T_{gap}}{273} \right)^{1.2405} (0.101/P_{gap})} \quad (3)$$

where $a_0 = 8.6 \times 10^{-3} \text{ m}^{0.5} \text{ MPa}^{-0.5}$, k_m and k_f are the harmonic mean thermal conductivity of the solids and the thermal conductivity of the gas in the gap, respectively, $P_i = Y_s t_s / r_{si}$ is the interfacial pressure between the fuel and the sheath surfaces (MPa), $R_{rms} = \sqrt{(R_1^2 + R_2^2)}/2 = 0.8 \mu\text{m}$ is the root-mean-square roughness of the two surfaces, R_1 and R_2 , and $H = 4.4 Y_s$ is the Meyer hardness of the Zircaloy sheath (MPa) as a function of the yield strength of the sheath Y_s , given in Section 3. The terms t_s and r_{si} refer to the sheath thickness, and inner radius, respectively, t_g is the gap thickness, g is the temperature jump distance for helium (for intact fuel), and T_{gap} and P_{gap} are the average gap temperature and pressure, respectively. The temperature at the sheath outer surface is dependent on heat transfer from the coolant:

$$T_{so} = T_c + \frac{P_{lin}}{2\pi r_{so} h_{sc}} \quad (4)$$

Here T_c is the coolant temperature, r_{so} is the sheath outer radius, and h_{sc} is the sheath-to-coolant heat transfer coefficient ($5 \times 10^4 \text{ W m}^{-2} \text{ K}^{-1}$).



2.1.2 Fission Gas Diffusion and Grain Growth

The fission gas diffusion and release is simulated by treating Xenon as the stable diffusing species. The release rate to the fuel grain surface is governed the Booth diffusion equation, which approximates the grains as spheres, as solved analytically by Kidson [7]. For a single power cycle, the Kidson solution reduces to that of Beck [8]:

$$\dot{R}_g = \dot{B} - \left(\frac{6\dot{B}}{\pi^2} \right) \sum_{n=1}^{\infty} (1/n^2) \exp(-n^2 \pi^2 D_g t / (d_g/2)) \quad (5)$$

where \dot{B} is the production rate of fission gas atoms, which is given as a function of the fission rate \dot{F} to be $0.251 \dot{F}$ [9], D_g is the gas diffusion coefficient in the uranium dioxide grain, and d_g is the grain diameter, given by Khoruzii et. al. [10] as:

$$\frac{dd_g}{dt} = k_g \left(\frac{1}{d_g} - \frac{1}{d_{g,max}} - \frac{\dot{F}T}{6.71 \times 10^{18} \exp(-5620/T)} \right) \quad (6)$$

where k_g is the grain growth rate term, and $d_{g,max}$ is the limiting grain size. The last term, where \dot{F} is the fission rate, accounts for the retarding effect of irradiation on grain growth. As fission gas atoms are released to the fuel grain surface, they form lenticular bubbles along the grain boundaries. Upon grain surface saturation, these bubbles percolate to form a diffusion path to the fuel surface. The pellet release is thus given by the volumetric integral of:

$$R_p = \begin{cases} \int R_g - \frac{1.736 \times 10^{22}}{T} \frac{6}{a_g} dV, & R_g \geq \frac{1.736 \times 10^{22}}{T} \frac{6}{a_g} \\ 0, & R_g < \frac{1.736 \times 10^{22}}{T} \frac{6}{a_g} \end{cases} \quad (7)$$

where R_g represents the number of atoms released from the grains as determined from the rate in Equation 5 and the term $\frac{1.736 \times 10^{22}}{T} \frac{6}{a_g}$ accounts for fission gas saturation on the grain surface [5].

2.1.3 Fuel Pellet Deformation

The strain in the fuel is a sum of thermal strain (ϵ_{th}) [11], densification strain (ϵ_{dens}) [12], gaseous fission product swelling (ϵ_{FG}) [13], and solid fission product swelling (ϵ_{FS}) [9]. These strains are:

$$\epsilon_{UO_2} = \epsilon_{th} + \epsilon_{dens} + \epsilon_{FG} + \epsilon_{FS} \quad (8)$$

$$\epsilon_{th} = \begin{cases} 0.99734 + 9.802 \times 10^{-5} T - 2.705 \times 10^{-10} T^2 + 4.391 \times 10^{-13} T^3, & 273K \leq T < 923K \\ 0.99672 + 1.179 \times 10^{-5} T - 2.429 \times 10^{-9} T^2 + 1.219 \times 10^{-12} T^3, & T \geq 923K \end{cases} \quad (9)$$

$$\epsilon_{dens} = 0.6 - \exp(-0.506 - 8.67 \times 10^{-10} T^3 (1 - \exp(-2.867 \times 10^{-2} \beta))) \quad (10)$$

$$\dot{\epsilon}_{FG} = \frac{1}{3} 8.8 \times 10^{-56} (2800 - T)^{11.73} \exp(-0.0162(2800 - T)) \times \exp(-8 \times 10^{-27} \beta) \frac{\partial \beta}{\partial t} \quad (11)$$

$$\epsilon_{FS} = \frac{1}{3} 0.0032 \beta \quad (12)$$

where β is the fuel burnup, determined by:

$$\frac{d\beta}{dt} = \frac{P_{lin} M_{UO_2}}{\pi \cdot a_p^2 \rho_0 M_U} \quad (13)$$



Here M_{UO_2} and M_U are the atomic masses of uranium dioxide and uranium, respectively, and ρ_0 is the as-fabricated density of uranium (10.7 g cm^{-3}). Given a change in the fuel radius from an initial $a_{p,in}$ to a_p , the change in fuel volume is equal to:

$$\Delta V_f = \pi(a_p^2 - a_{p,in}^2) \cdot l \quad (14)$$

where l is the length of the fuel element.

2.1.4 Sheath Deformation

The thin sheath (inner-radius-to-wall-thickness ratio greater than 10) experiences deformation due to external coolant pressure and internal fuel expansion. The sheath deformation is a function of the hoop strain (ε_s^θ) [14]:

$$r_{si} = r_{si,init} \cdot \varepsilon_s^\theta \quad (15)$$

The hoop strain is the sum of thermal (ε_{th}^θ) [5], elastic (ε_{el}^θ) [14], and creep [15] strains (ε_{cr}^θ) given by:

$$\varepsilon_s^\theta = \varepsilon_{th}^\theta + \varepsilon_{el}^\theta + \varepsilon_{cr}^\theta \quad (16)$$

$$\varepsilon_{th}^\theta = \begin{cases} -2.073 \times 10^{-3} + 6.721 \times 10^{-6} T, & T < 1050 \text{ K} \\ 1.486 \times 10^{-2} - 9.398 \times 10^{-6} T, & 1050 \text{ K} \leq T < 1270 \text{ K} \\ -9.450 \times 10^{-3} + 9.7 \times 10^{-6} T, & T \geq 1270 \text{ K} \end{cases} \quad (17)$$

$$\varepsilon_{el}^\theta = \frac{1}{E_{Zr}} \frac{r_{si}}{t_s} (P_{in} - P_{ex}) \left(1 - \frac{\nu_{Zr}}{2}\right) \quad (18)$$

$$\varepsilon_{cr}^\theta = \varepsilon_{cr} \frac{F - \frac{G}{2}}{\sqrt{\frac{F+G}{4} + H}} \quad (19)$$

where E_{Zr} , ν_{Zr} , F , G , and H represent the Young's modulus, Poisson's ratio, and Hill anisotropy parameters for the sheath, respectively. The external coolant pressure P_{ex} is equal to 10.7 MPa, and the internal pressure can be determined using the ideal gas law:

$$P_{in} = P_{gas} = \frac{(n_{He} + n_{FG}) RT_{gap}}{N_{av} (V_{cracks} + V_{gap})} \quad (20)$$

where n_{He} is the number of helium atoms initially in the fuel-to-sheath gap, n_{FG} is the number of fission gas atoms released and is equal to R_p as determined in Section 2.1.2. The terms N_{av} , R , and T_{gap} represent Avogadro's number, the ideal gas constant, and the average temperature in the fuel-to-sheath gap, respectively. The molar gas density is simply the total number of moles divided by the total volume in Equation 20 above; i.e.: $(n_{He} + n_{FG}) / (N_{av} [V_{cracks} + V_{gap} + V_{dishes}])$. The volume occupied by the gas is the sum of the volume of the fuel cracks (V_{crack}), fuel-to-sheath gap (V_{gap}) and the inter-pellet dishes (V_{dish}). The crack volume is equal to the change in volume due to fuel deformation (ΔV) as determined in Section 2.1.3. The dish volume is approximated assuming a dish depth determined by linear thermal expansion at the fuel centerline using the thermal strain of Equation 9. The gap volume is a function of the distance left between the fuel and sheath due to their respective deformations:



$$V_{gap} = \pi(r_{si}^2 - a_p^2) \cdot l \quad (21)$$

Finally, the creep strain (ε_{cr}) in Equation 19 is the sum of the strains due to dislocation glide (ε_d) and grain boundary glide (ε_g) as given by [16]:

$$\dot{\varepsilon}_{cr} = \dot{\varepsilon}_d + \dot{\varepsilon}_g \quad (22)$$

$$\dot{\varepsilon}_d = 1.88 \times 10^{-2} \exp\left(-\frac{34726}{T}\right) \left(\frac{r_{si}}{t_s} (P_{in} - P_{ex}) - \sigma_i\right)^{5.3} \quad (23)$$

$$\dot{\varepsilon}_g = 6.34 \times 10^{-6} \left(\frac{1}{G_s d_{g,Zr}} \frac{r_{si}}{t_s} (P_{in} - P_{ex})\right)^2 \exp\left(-\frac{9431}{T}\right) \quad (24)$$

where G_s is the shear modulus of the sheath. The term $d_{g,Zr}$ represents the grain size of Zircaloy-4, and the term σ_i represents the internal stress field given by [16]:

$$\dot{\sigma}_i = 0.016 E_{Zr} \dot{\varepsilon}_d \left(1 - \sigma_i \left[0.33 \left(10^{-6} \cdot \frac{r_{si}}{t_s} (P_{in} - P_{ex}) - \sigma_i\right)\right]^{-1}\right) \quad (25)$$

2.2 Element Bowing Model

The bowing equation, based on the principle of virtual work [17] is:

$$\delta W = \delta \int_V (-\varepsilon_{el} \sigma + \mathbf{u}^T \mathbf{F} dV) = 0 \quad (26)$$

where \mathbf{F} is the force vector on the beam known from the external loads, \mathbf{u} is the displacement vector (m), ε_{el} is the elastic strain and σ is the internal stress of the beam (MPa). The long and slender geometry of a fuel element allows a beam approximation, i.e. there is no deformation that occurs in the cross section but an applied force causes lateral deflection (deformation) from the body's central axis and torsion of the cross section [17]. The same assumption was made by AECL and MARTEC in their treatment of an element deformation model [1]. This approach allows Equation 26 to be expressed as a line integral as shown in Equation 27. Here the external forces and the internal strain are described by the bending moments in each axis (M_x, M_y, M_z), the torsion of each axis ($\theta_x, \theta_y, \theta_z$), the force acting perpendicular to the cross section (N), and the displacement of the centroid of the cross section (u_{axi}) (the path of the cross sections centroids through body makes up the body's central axis).

$$\delta W = \int_L \left(M_y \left(\frac{\partial \theta_y}{\partial s}\right) + M_z \left(\frac{\partial \theta_z}{\partial s}\right) M_x \left(\frac{\partial \theta_x}{\partial s}\right) + N \left(\frac{\partial u_{axi}}{\partial s}\right) \right) dx \quad (27)$$

Due to the construction of a fuel element consisting of the fuel pellets and sheath, by assuming the pellets can be represented as one cylinder the element can be viewed as two separate beams which undergo bending based on their individual material properties. However, because the sheath encases the pellets, the total bending of the element is then the summation of the bending of both the sheath and the pellets:

$$M^e = M^s + A \times M^p \quad (28)$$



Here M is the total bending moment and the superscripts e , s and p refer to the element, sheath and pellet, respectively, and A is a fitting parameter to experimental data that is less than one.

2.3 Out-Reactor Fuel Oxidation Simulation

A conceptual model of Higgs et. al. [6] was developed to mechanistically describe fuel oxidation behaviour in defective fuel elements. This model is adapted in this work and subsequently modified to represent an inner-surface heated and unirradiated fuel element in an out-reactor loop experiment at the Stern Laboratories. This experiment is specifically planned to help validate the fuel oxidation model where the experimental conditions can be well-controlled. In particular, this experiment provides an opportunity to measure the fuel element temperature in an instrumented element with continued fuel oxidation for normal temperature and pressure CANDU coolant conditions. A post-test analysis also provides an opportunity to assess the fuel oxidation end-state of the element. Currently, the mechanistic model of Higgs is adapted to help design the loop test and assess the amount of fuel oxidation expected for a one and two week experiment.

In the Higgs mechanistic model, a treatment is considered for both gas phase and solid-state diffusion, which are controlled by temperature-dependent reactions. Hydrogen (H_2) and steam (H_2O) are specifically considered in the model for the out-reactor experiment. Figure 1 depicts an axial cross section of a test fuel element.

Cracks appear in the fuel pellets due to fuel thermal expansion [18,19]. Below the elastic-plastic boundary, cracks will initially appear but will later self heal [9,20]. This transition is assumed to occur at a temperature of 1523 K, though in reality it occurs over a range of temperatures [9]. Figure 1 depicts a deliberate sheath defect which is 1 mm wide (into the page) and 20 mm long in the axial z -direction, with a possible gap between two pellets under the defect site.

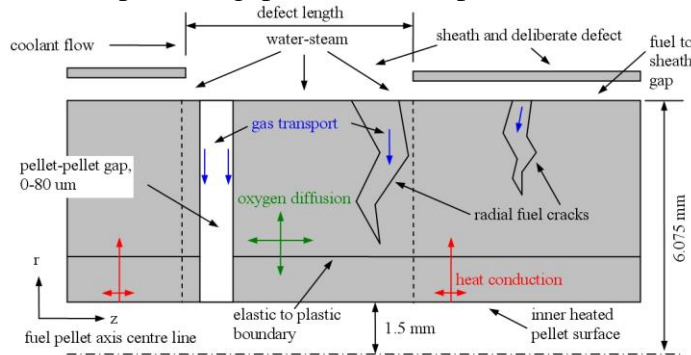


Figure 1: A 2D z - r representation of test fuel pellet.

The generalized mass balance equation for oxygen transport in the fuel matrix is given by Equation 29:

$$c_u \frac{\partial x}{\partial t} = c_u \nabla \cdot \left(D \left(\nabla x + x \frac{Q}{RT^2} \nabla T \right) \right) + \sigma_f R_f^{react} \quad (29)$$

where D is the diffusion coefficient of oxygen interstitials as a function of temperature. x is the



oxygen deviation from stoichiometry in the uranium oxide matrix (UO_{2+x}), c_u is the molar density of uranium, R is the universal gas constant, T (K) is temperature, σ_f is the pellet average ratio of crack area to fuel volume, and Q is the molar effective heat transport. The kinetic reaction rate, R_f^{react} , for fuel oxidation in moles O or $\text{H}_2 \text{ m}^{-2} \text{ s}^{-1}$ is

$$R_f^{react} = c_u \alpha \sqrt{(1-q)p_t} (x_e - x) \quad (30)$$

where α is the rate coefficient for the surface-exchange of oxygen at the pellet surface, p_t is the total system pressure of 100 atm, q is the hydrogen mole fraction, x is stoichiometric deviation, and x_e is the equilibrium stoichiometry deviation based on the local oxygen potential of the gas in the fuel cracks [6]. Hydrogen is contributed to the gas environment in the fuel cracks by the fuel-oxidation reaction. The cracked fuel is assumed to have a porosity P (ε in Equation 31). The mass balance for the hydrogen molar concentration, qc_g , in the fuel cracks is given by Equation 31, where c_g is the total molar concentration of the gas and cD_g is the steam diffusivity quantity.

$$\varepsilon \frac{d(qc_g)}{dt} = \varepsilon \nabla \cdot (cD_g \nabla q) + \sigma_f R_f^{react} \quad (31)$$

Equation 31 is applicable only in the domain above the elastic-plastic boundary and only under the defect site (see dashed lines in Figure 1). For out-reactor analysis, the temperature in the fuel is determined by Equation 1 setting the heat generation term to zero and setting a boundary condition at the inner surface of the fuel based on the heating element at the centre.

3. Material Properties and Operating Conditions

The material properties for the components of CANDU fuel are fully discussed in Ref. 5 and Ref. 6. Typical operating conditions for a CANDU fuel element are listed in Table 1.

Table 1 Typical operating conditions for CANDU fuel

Term	Description	Expression	Units
P_{lin}	Linear element rating	20 to 65	kW m ⁻¹
T_c	Bulk coolant temperature	550 to 580	K
β	Burnup	0 to 235	MWh kgU ⁻¹

The properties and parameters of the gap, cracks, and dishes are given in Table 2.

Table 2 Properties of intra-element space

Term	Description	Expression	Units
ρ_{He}	Density of helium at STP	44.65	mol He m ⁻³
ρ_{Xe}	Density of xenon at STP	43.66	mol Xe m ⁻³
C_p	Heat capacity	20.786	J mol ⁻¹ K ⁻¹
k_{He}	Thermal conductivity of helium	$15.8 \times 10^{-4} T^{0.79}$	W m ⁻¹ K ⁻¹
k_{Xe}	Thermal conductivity of xenon	$4.351 \times 10^{-3} T^{0.8616}$	W m ⁻¹ K ⁻¹
n_{He}	# of He atoms in gap	3.483×10^{19}	atoms
$g_{t,lin}$	Initial gap thickness	5×10^{-5}	M
g	Temperature jump distance	8×10^{-6}	M
c_g	Total molar concentration of gas in defective fuel	p_t / RT	mol m ⁻³
$c_g D_g$	Chapman-Enskog diffusion term	$2.2646 \times 10^{-3} \left(\sqrt{T (M_{H_2}^{-1} + M_{H_2O}^{-1})} / \sigma_{AB}^2 \Omega_{AB} \right)$	mol m ⁻¹ s ⁻¹

The fuel material properties are summarized in Table 3.



Table 3 Material properties of UO₂ fuel

Term	Description	Expression	Units
D	Diffusion coefficient of oxygen in UO ₂	$(2.5 \times 10^{-4}) \exp(-16400/T)$	m ² s ⁻¹
Q^*	Heat of transport of oxygen in UO ₂	$-3.5 \times 10^{34} \exp(-17(4+2x))$	J mol ⁻¹
σ_{fuel}	Surface-area-to-volume ratio of UO ₂	$\begin{cases} 908, T < 1473K \\ 908 \times (0.0025T - 3.6825), 1473K \leq T \leq 1873K \\ 0, T > 1873K \end{cases}$	m ⁻¹
α	Oxidation surface exchange coefficient	$0.365 \exp(-23500/T)$	m s ⁻¹
c_u	Molar density	$4.1 \times 10^4 \rho_{UO_2}$	mol U m ⁻³
ρ_{UO_2}	Density	$10960 \cdot \varepsilon_{th}^{-3} (1-P)$	kg m ⁻³
P	Fuel porosity	$0.0282(1 - \varepsilon_{dens})$	-
C_p	Heat capacity ($x=0$ for intact fuel)	$52.1743 + 45.8056x + (87.951 \times 10^{-3} - 7.3461 \times 10^{-2}x)T$ $+ (1-x) \{ -84.2411 \times 10^{-6} T^2 + 31.542 \times 10^{-9} T^3 - 2.6334 \times 10^{-12} T^4 \}$ $- (713910 + 295090x) T^{-2}$	kJ mol ⁻¹ K ⁻¹
k_{UO_2}	Thermal conductivity (intact fuel)	$\left[\frac{1-P}{1+(6.5-0.00469T)P} \right]$ $\times \left[\frac{(297.7(535.285)^2/T^2 (\exp[533.285/T]-1)^2) \exp[533.285/T]}{(0.339+0.06867T^m)(1+3\varepsilon_{th})} \right]$ $+ 5.2997 \times 10^{-3} T \exp[-13358/T] \{ 1+0.169[13358/T+2]^2 \}$	kW m ⁻¹ K ⁻¹
k_{UO_2+x}	Thermal conductivity (defective fuel)	$\kappa_{1d} \kappa_{1p} \kappa_{2p} \kappa_{4r} k_{2+x}$	kW m ⁻¹ K ⁻¹
κ_{1d}	Factor for dissolved fission products	$\left(\frac{1.09}{\beta^{3.265}} + \frac{0.0643}{\sqrt{\beta}} \sqrt{T} \right) \arctan \left(\frac{1}{1.09/\beta^{3.265} + (0.0643/\sqrt{\beta})\sqrt{T}} \right)$	-
κ_{1p}	Factor for precipitated fission products	$1 + \frac{0.019\beta}{(3-0.019\beta)(1+\exp\{-(T-1200)/100\})}$	-
κ_{2p}	Factor for porosity effects	$(1 - (2.6 - 0.5 \times 10^{-3}T)P)$	-
κ_{4r}	Factor for radiation effects	$1 - \frac{0.2}{1 + \exp\{(T-900)/80\}}$	-
k_{2+x}	Uncorrected thermal conductivity of UO ₂	$k_{ph} + k_e$	kW m ⁻¹ K ⁻¹
k_{ph}	Phonon contribution to thermal conductivity	$(A + BT)^{-1}$	kW m ⁻¹ K ⁻¹
A	Phonon-phonon interaction term	$14 - 10.763x^{0.5} - 2381.4x + 12819.86x^{1.5}$	K m kW ⁻¹
B	Phonon-polaron interaction term	$\begin{cases} 0.2218 + 0.2562\sqrt{x} - 0.64x - 3.6764(\sqrt{x})^3, x < 0.155 \\ 0, x \geq 0.155 \end{cases}$	m kW ⁻¹
k_e	Polaron contribution to thermal conductivity	$(0.87 + 2.5 \times 10^{-5}T)^{-1} \frac{2.024 \times 10^8}{T^{5/2}} \exp(-16350/T)$	kW m ⁻¹ K ⁻¹
κ	Neutron diffusion length	$89.89 + 0.6\beta^{0.68}$	m ⁻¹
D_g	Diffusion coefficient for fission gas in UO ₂	$\frac{5.711 \times 10^{-4} \cdot F \cdot D_{i1} \cdot D_{i2}}{\left(\frac{2.432 \times 10^7 \cdot 5 \times 10^{-10} + 5.3 \times 10^{-8} \exp[-8702.7/T]}{D_{i1}} D_{i2} \right) + 5.711 \times 10^{-4} \cdot F \cdot D_{i1}}$	m ² s ⁻¹
D_{i1}	Term included in diffusion coefficient	$D_{i1} = (1.5 \times 10^{-9} + 5.3 \times 10^{-8} \exp[-8702.7/T])^2$	-
D_{i2}	Term included in diffusion coefficient	$D_{i2} = 7.6 \times 10^{-9} \exp[-35225.443/T] + 2.372 \times 10^{-8} \exp[-27780/T] \cdot D_{i3}$ $\times \left\{ \left[1 + 8.167 \times 10^{-34} \frac{F}{\exp[-27780/T] \cdot D_{i3}^2} \right]^{0.5} - 1 \right\} + 8 \times 10^{-40} F$	-
D_{i3}	Term included in diffusion coefficient	$D_{i3} = 1.186 \times 10^{-4} + 100 \exp[-27780/T]$	-
$d_{g,in}$	Initial grain radius	1.14×10^5	M
k_g	Grain growth rate term	$1.46 \times 10^{-8} \exp(-32100/T)$	m ² s ⁻¹
$d_{g,max}$	Limiting grain size	$2.23 \times 10^{-3} \exp(-7620/T)$	M
E_{UO_2}	Young's modulus	$2.33 \times 10^{11} \cdot (1 - 2.752[1 - \varepsilon_{th}(1-P)]) \cdot (1 - 1.0915 \times 10^{-4} \cdot T)$	Pa
ν_{UO_2}	Poisson's ratio	0.316	-



The material properties of the sheath are listed in Table 4.

Table 4 Properties of the Zircaloy-4 fuel sheath

Term	Description	Expression	Units
ρ	Density	$71805.292(1 + (\Delta L/L_0)_{ax})(1 + (\Delta L/L_0)_d)$	mol m ⁻³
$(\Delta L/L_0)_{ax}$	Axial thermal expansion term	$-2313.4 + 9.5043T - 7.0469 \times 10^{-3}T^2 + 3.6644 \times 10^{-6}T^3$	-
$(\Delta L/L_0)_d$	Diametral thermal expansion term	$-2585.8 + 10.142T - 4.8362 \times 10^{-3}T^2 + 2.2058 \times 10^{-6}T^3$	-
C_p	Heat capacity	$23.324 + 8.2402 \times 10^{-3}T + 11.6313 \times 10^{-7}T^2$	J mol ⁻¹ K ⁻¹
k	Thermal conductivity	$7.51 + 2.09 \times 10^{-2}T - 1.45 \times 10^{-5}T^2 + 7.67 \times 10^{-9}T^3$	W m ⁻¹ K ⁻¹
E_{Zr}	Young's modulus	$1.148 \times 10^{11} - 6 \times 10^7 T$	Pa
ν_{Zr}	Poisson's ratio	0.32	-
F, G, H	Hill's anisotropy parameters	0.773, 0.532, 0.195	-
$r_{si,in}$	Initial sheath inner radius	0.006145 or 0.00722	M
$t_{s,in}$	Initial sheath thickness	4×10^{-4}	M
d_g	Grain diameter	3×10^{-6}	M
Y_s	Yield Strength	$Y_s = 148695 - 136.65(\overline{T_{sheath}})$	MPa

By running the fuel performance model using these parameters (Section 4), it is possible to compare the model predictions to pre-existing data from fuel performance simulations and experimental data.

4. Numerical Implementation

The equations outlined in Section 2, given the material properties and operating conditions listed in Section 3, are solved using the commercial platform COMSOL MultiphysicsTM (henceforth 'Comsol') [21]. In Comsol, systems of differential equations are solved on a meshed geometry using the finite element method.

For the intact fuel element performance model, the two-dimensional geometry is divided into two domains, representing the fuel and sheath. A moving mesh is used such that the geometry expands and contracts according to the deformation equations outlined in Section 2.1. The heat conduction equation in Section 2.1.1 is solved in both domains; however, the source term accounting for heat generation due to fission is included only in the fuel domain.

The model is able to describe the gap dynamics with the possibility of sheath closure. The mixed-gas phase and solid-to-solid heat transfer that occurs during contact of the rough surfaces of the fuel and sheath is simulated as conduction through a 1- μ m thermally resistive layer (i.e., equal to the surface roughness) using the 'Identity Pairs' feature of Comsol. The total heat transfer coefficient given pellet-sheath contact is equal to $h_{solid} + h_{gas}$, the sum of the solid and gas heat transfer coefficients given in Equations 2 and 3, respectively. The ratio of this new gap heat transfer coefficient to the original gas heat transfer coefficient is used to scale the gas thermal conductivity to a new effective thermal conductivity:

TM COMSOL Multiphysics is a trademark of Comsol AB.



$$k_{eff} = \frac{h_{solid} + h_{gas}}{h_{gas}} k_f \quad (32)$$

The fission gas diffusion equations in Section 2.1.2 are solved in the fuel domain. Also in the fuel domain, the fuel strain functions in Section 2.1.3 are entered into a pre-built ‘Axial Stress-Strain’ application mode in Comsol, which solves for the fuel deformation using internal functions. In the high temperature plastic region of the fuel, the deformation u_p is determined by:

$$\rho_{UO_2} \frac{\partial^2 u_p}{\partial t^2} + \frac{\partial u_p}{\partial r} = \varepsilon_{UO_2} \quad (33)$$

where ρ_{UO_2} is the density of UO_2 and ε_{UO_2} is given by Equation 8. The sheath deformation equations in Section 2.1.4 are applied to the sheath domain.

In the oxidation model, a weak form of the differential equations can be used to account for physical phenomena in the pellet-pellet gap, where σ and P take on different values, that apply to a surface, as a more robust technique [22]. Hence, the oxygen transport in the fuel matrix, Equation 29, and the gas diffusion, Equation 31, can be recast as an equality of integrals, thereby reducing the order of the equations by one degree. This is accomplished by integration by parts using the divergence theorem to produce:

$$\varepsilon_{ppg} g \int_{\Omega} \frac{\partial u}{\partial t} V d\Omega = \int_{\Omega} (\varepsilon_{ppg} \nabla V \cdot \Gamma + VF) d\Omega - \varepsilon_{ppg} \int_{\partial\Omega} V(\Gamma \cdot n) ds \quad (34)$$

Here, V is a test function. Substituting $\sigma_{ppg} R_f^{react}$, $cD_g \nabla q$, c_g , and q for F , Γ , g and u respectively, and noting that the constraint term $\varepsilon_{ppg} \int_{\partial\Omega} V(\Gamma \cdot n) ds$ goes to zero, a weak form of the equations is developed that can be solved in Comsol.

5. Results and Discussion

The results of the models for the intact fuel performance code, fuel element bowing analysis and out-reactor defective fuel element simulation are described in the following sections.

5.1 Intact fuel element performance model

The results of the intact fuel performance model are compared to those of the industry-standard toolset ELESTRES, as reported in Ref. 5, and the industry-produced code ELESIM, run for the same conditions. As seen in Figure 2 below, the Comsol model predictions show similar agreement with the ELESTRES and ELESIM codes at different linear power fuel ratings. A small exception is at 40 kW m⁻¹, where a slight increase in gas pressure is predicted by the Comsol code near the end of the fuel lifetime, implying that grain boundary saturation may be reached at this point. The release of fission product gases to the fuel-to-sheath gap, which degrades the fuel-to-sheath thermal conductivity, also explains why the temperature predictions of the Comsol treatment are slightly higher than those of both ELESTRES and ELESIM at 40 kW m⁻¹.

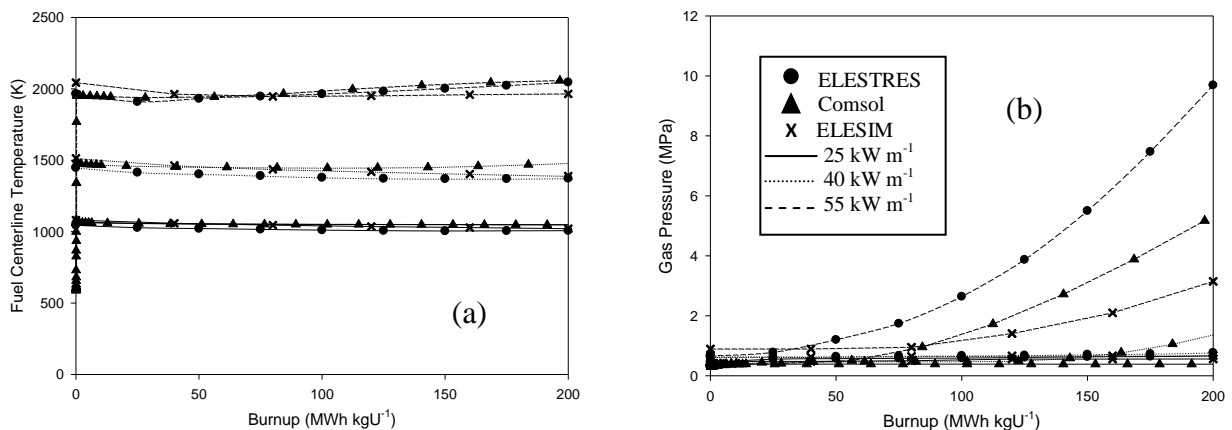


Figure 2 Comparison of (a) centerline temperature and (b) internal gas pressure predictions of the current treatment to the ELESTRES and ELESIM codes. The legend applies to both figures.

The deformation models for the fuel and sheath can be assessed by comparing the sheath hoop strain predictions as shown in Figure 3 below. In this case, the predictions of a one-dimensional version of the Comsol model [23] are included.

While all four codes are in agreement at the different powers, it is clear that the two-dimensional model results at 25 kW m⁻¹ are different than those of the one-dimensional model, with the discrepancy decreasing at 40 kW m⁻¹ and becoming negligible at 55 kW m⁻¹. As discussed in Section 4, the two-dimensional model makes use of Comsol's pre-built stress-strain application mode for low-temperature deformation, whereas the one-dimensional model uses the equations of Morgan [5]. For plastic deformation at high temperatures, both models use Equation 33, which explains the closer agreement between the two models with increasing power.

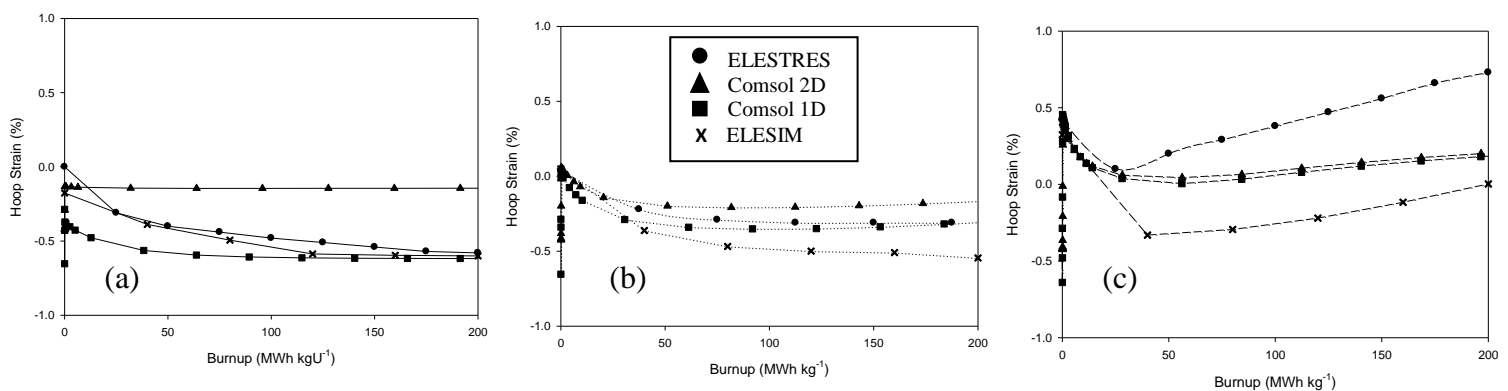


Figure 3 Comparison of hoop strain predictions of the current treatment in one and two dimensions to the ELESTRES and ELESIM codes at (a) 25 kW m⁻¹, (b) 40 kW m⁻¹, and (c) 55 kW m⁻¹.

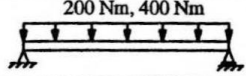
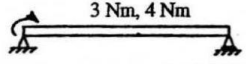
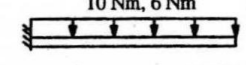
5.2 Fuel element bowing model

For the bowing model, comparisons to other simulations of fuel element deformation are made. Table 5 contains summaries of BOW verification cases from Yu, Tayal, and Singh [24], and Table 6 shows the maximum horizontal and vertical displacements as determined in Comsol.



The Comsol results are within the same tolerance of a 1% difference from the analytical results as for the BOW code.

Table 5: Verification of Yu, Tayal, and Singh results comparing the BOW code to theoretical calculations

Cases	Description of Cases*	Horizontal Direction			Vertical Direction		
		Theory	BOW	Difference	Theory	BOW	Difference
1	 200 Nm, 400 Nm	7.016	7.019	< 1%	14.03	14.04	< 1%
2	 3 Nm, 4 Nm	2.074	2.070	< 1%	2.771	2.760	< 1%
3	 10 Nm, 6 Nm	3.367	3.369	< 1%	2.020	2.021	< 1%

* The first load (moment) is applied horizontally; the second load is applied vertically

Table 6: Results of COMSOL model simulating conditions of Case 3 from Table 5

Max. Horizontal (mm)	3.368
Max. Vertical (mm)	2.021

5.3 Simulation of out-reactor defective fuel experiment

For the out-reactor loop test, the defective fuel element contains a central-heater element. The heat conduction and resultant temperature profile for this instrumented fuel element is modelled, and the subsequent fuel oxidation behaviour assessed for these fuel temperature conditions. Two 3-D model solutions are presented: (i) a model where the element contains a regular slit defect with just steam transport through the cracked fuel pellets and (ii) a similar model with a slit defect but where there is a possibility of steam ingress also between adjacent fuel pellets (directly under the defect site). A heating temperature of 1750°C at the UO₂ inner 3-mm diameter surface was selected for the given heater design. Figure 4 provides fuel oxidation results for a full-length fuel element that is 48-cm in length (24-cm long model) for these two cases, showing that the oxygen stoichiometric deviation decreases with distance from the defect.

Figure 4(a) shows that the stoichiometric deviation could be as high as UO_{2.016} near the defect site and near the heater element in one week of heating. This deviation rises to UO_{2.023} after two weeks of heating. Figure 4(b) shows that stoichiometric deviation could be as high as UO_{2.036} in one week, reaching UO_{2.047} in two weeks, when consideration of possible steam ingress in a pellet-pellet gap under the defect site is also made. Post-experiment techniques can provide oxygen potential values at various locations in the fuel test pellets to validate these predictions. With a 20-mm² sized defect after one week of heating, the current analysis suggests that coulometric titration could be used to identify this amount of oxidation with a sensitivity of $x = 0.01$ in the stoichiometric deviation for this technique [25].

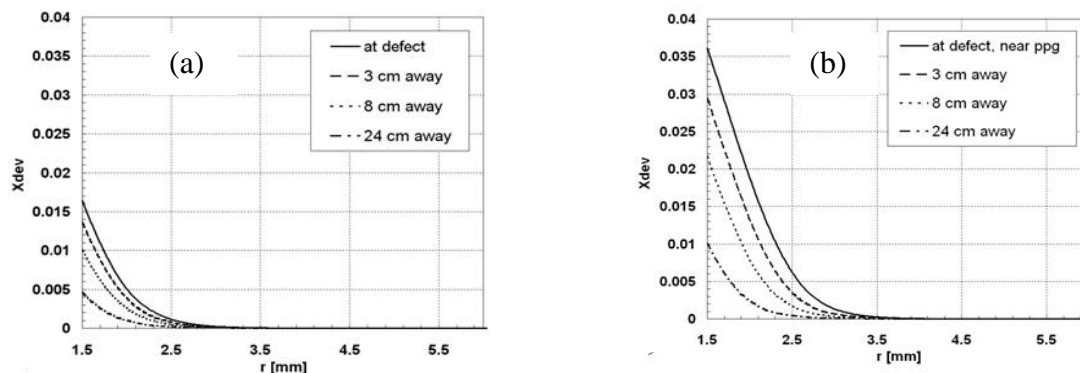


Figure 4: Oxygen stoichiometric deviation vs. radial position in the fuel pellet at several locations along a fuel element of length of 48 cm after one-week heating (a) without steam penetration between adjacent pellets and (b) with steam penetration between adjacent pellets.

Possible fuel oxidation at pellet-pellet surfaces, and other possible mechanisms, may help to explain the lower predictions of Higgs for 3-D simulations where a pellet-pellet gap path for steam penetration was not considered. It should be noted that with a 2-D model, defect sizes in the Higgs treatment [6] were modelled as circumferential rings with a thickness equal to the observed axial length of the defect, which is considerably larger than the actual physical size of the defect itself. Current work is continuing on the improvement of the 3-D model. The out-reactor experiments to be performed at Stern Laboratories will be used to specifically help benchmark the fuel-oxidation model.

6. Conclusions and Recommendations

The fuel performance model displays reasonable agreement with the results of the pre-existing codes, ELESTRES and ELESIM, in terms of temperature, gas pressure, and structural deformation. The fuel element bowing model, which agrees with the results of the BOW code, can be eventually linked to the fuel element performance code to describe the primary effect of thermally-induced element deformation. This model can also be extended further to account for element-element contact and end-plate effects in order to model the complete fuel bundle.

The predictions of the oxidation model demonstrate the need for a three-dimensional model to properly account for the effect of the actual defect geometry. Further consideration must also be given to the contribution of steam ingress into pellet-pellet clearances. From the results of the model, it is seen that increasing the heating duration by one week increases the maximum oxygen stoichiometric deviation by 30-44%, which is an important consideration in the design of the out-reactor experiment.

Future work will focus on integrating the intact fuel performance model and defective fuel oxidation model to produce a defective fuel performance code. Eventually, it is also hoped to include fuel deformation phenomena in this model with the ultimate intention to build a full fuel bundle model that accounts for bundle ageing effects under normal operation and bundle sag under high-temperature accident conditions.



7. References

- [1] M. Tayal, Nuclear Engineering and Design, 116 (1989) 149.
- [2] J. Veeder, M.H. Schankula, Nuclear Engineering and Design, 29, pp. 167-179, 1974.
- [3] B.J. Lewis, F.C. Iglesias, D.S. Cox, E. Gheorhiu, Nuclear Technology 92 (1990), 353.
- [4] D.R. Olander, *Nuclear Technology*, 74 (1986) 215.
- [5] D. Morgan, MAsc. Thesis, Royal Military College of Canada, 2007.
- [6] J.D. Higgs, B.J. Lewis, W.T. Thompson and Z. He, J. Nucl. Mater., 366 (2007) 99.
- [7] G.V. Kidson, J. Nucl. Mater. 88 (1980) 299.
- [8] S.D. Beck, Battelle Memorial Institute, Report No. BMI-1433, 1960.
- [9] D.R. Olander, *Fundamental Aspects of Nuclear Reactor Fuel Elements*, TID-26711-p1, US. Department of Energy, 1976.
- [10] O.V. Khoruzhii, S.Yu. Kourtchatov, V.V. Likhanskii, J. Nucl. Mater. 265 (1999), 112.
- [11] D.G. Martin, J. Nucl. Mater. 152 (1988), 94-101.
- [12] I.J. Hastings, L.E. Evans, Journal of the American Ceramics Society 62 (1979), 217-218.
- [13] D.T. Hagerman, ed., MATPRO—A Library of Materials Properties for Light-Water-Reactor Accident Analysis, SCDAP/RELAP5/Mod 3.1 Code manual, NUREG/CR-6150 Vol. 4. (1997).
- [14] R.C. Hibbeler, *Mechanics of Materials*, Prentice Hall, Upper Saddle River, New Jersey, 2000.
- [15] M.F. Ashby, Acta Metallurgica 887 (1972), 20.
- [16] H.E. Sills, R.A. Holt, Zirconium in the Nuclear Industry (Fourth Conference), ASTM STP 681, American Society for Testing and Materials, 1979, 325-341.
- [17] K. D. Hjelmstad, *Fundamentals of Structural Mechanics*, Prentice-Hall, 1997.
- [18] M. Oguma, Nuclear Engineering and Design, 76 (1983) 35.
- [19] Y. Sumi, L.M Keerand, and S. Nemat-Nasser, J. Nucl. Mater. 96 (1981) 147.
- [20] C. Bernaudat, Nuclear Engineering and Design 156 (1995) 373.
- [21] COMSOL Multiphysics Version 3.5a finite element modeling and simulation commercial software, www.comsol.com.
- [22] William B.J. Zimmerman, Multiphysics Modelling with Finite Element Methods, World Scientific Publishing Co. Pte. Ltd., London, 2006.
- [23] K. Shaheen, and B.J. Lewis, Proceedings of the 2009 Topfuel Conference.
- [24] S.D. Yu, M. Tayal, P.N. Singh, Proceedings of the Fourth International Conference on CANDU Fuel, October 1-4, 1995, 364-375.
- [25] R.A. Verrall, Z. He and J. Mouris, J. Nucl. Mater. 344 (2005) 240-245.

Acknowledgements

The authors would like to acknowledge J. Higgs, and D. Morgan for their pioneering work on Comsol modelling of defective fuel oxidation and intact fuel performance, respectively. The authors also thank B. Leitch and A. Williams of Chalk River Laboratories for sharing their expertise on finite element modelling and fuel performance codes, and C. Thiriet of Chalk River Laboratories and G. Hadaller of Stern Laboratories for their guidance in adapting the oxidation model for the upcoming out-reactor experiment.